An Optically Driven Bistable Janus Rotor with Patterned Metal Coatings

Yiwu Zong,[†,§] Jing Liu,[‡,§] Rui Liu,[†] Honglian Guo,[*,‡,#] Mingcheng Yang,[†] Zhiyuan Li,[‡] and Ke Chen[*,†]

[†]Beijing National Laboratory for Condensed Matter Physics and Key Laboratory of Soft Matter Physics, Institute of Physics, Chinese Academy of Sciences, Beijing 100190, China and [‡]Beijing National Laboratory for Condensed Matter Physics and Key Laboratory of Optical Physics, Institute of Physics, Chinese Academy of Sciences, Beijing 100190, China. [§]Y.Z. and J.L. contributed equally to the work. [#]Present address: School of Physics, South China University of Technology, Guangzhou 510640, China.

ABSTRACT Bistable rotation is realized for a gold-coated Janus colloidal particle in an infrared optical trap. The metal coating on the Janus particles are patterned by sputtering gold on a monolayer of closely packed polystyrene particles. The Janus particle is observed to stably rotate in an optical trap. Both the direction and the rate of rotation can be experimentally controlled. Numerical calculations reveal that the bistable rotation is the result of spontaneous symmetry breaking induced by the uneven curvature of the coating patterns on the Janus sphere. Our results thus provide a simple method to construct large quantities of fully functional rotary motors for nano- or microdevices.

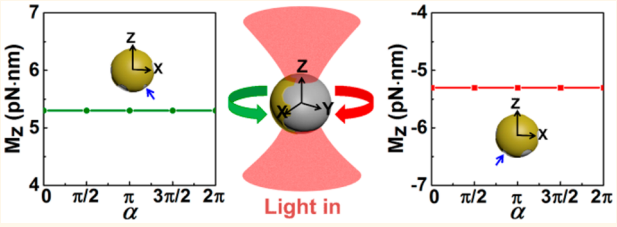

KEYWORDS: microrotor · Janus particles · optical traps · spontaneous symmetry breaking · controlled rotation

Linear and rotary motors are the basic components in mechanical machineries that are crucial to industrialized societies. On the molecular scale, many cell functions in living organisms are driven by similar biological motors, from cargo transportation,[1,2] gene regulation[3,4] to muscle contractions.[5,6] Synthetic motors that can reliably work on the nano- and micrometer scales have been pursued by researchers, for their great potential in biomedicine, material science and nanotechnology.[7−26] Self-propelled microswimmers[7,8,10,14,15,19,20] and microrotors driven by external electric[21−23] or magnetic fields[17,24−26] have been reported recently. Among proposed driving mechanisms, laser light, that carries both linear and angular momentum, is a promising tool to generate rotation in microdevices.[27−29] For instance, angular momentum can be transferred from an elliptically polarized laser beam to a birefringent particle, generating a mechanical torque.[30−33] The rotational direction of the particle can be switched by modulating the laser polarization conditions.[34] Precisely fabricated asymmetric devices such as microturbines[35] or gammadion shaped microrotors[36,37] can be rotated by linearly polarized light. The rotational directions of these devices, however, are generally determined by the geometric bias of the rotor and, thus, do not allow free switching, with the exception of plasmonically driven rotors whose rotational directions can be reversed by switching the laser wavelengths.[36] So far, all reported light-driven rotors require complex manipulation of either the illuminating laser and/or the structure and materials of the device, which has limited their areas of applications. A microrotor that allows flexible control of both the direction and rate of rotation and at the same time is easy to produce *en masse* would expand the scope of its utility in practice.

Janus spheres that have different optical properties on the two hemispheres are potential candidates for optical rotors.[38,39] One particular advantage of Janus particles is that they can be easily produced in large quantities, to the order of millions in a single batch. Controlling of the optical property distribution in a Janus sphere is critical to the design of a functional rotor. For the simplest case, a Janus particle with a flat circular boundary line between the coated and uncoated surfaces cannot stably rotate, as the system symmetry is not biased toward one rotational direction or the other. Such particles are observed to rotate intermittently in an optical trap, with frequent

* Address correspondence to kechen@iphy.ac.cn, phhlguo@scut.edu.cn.

Received for review June 12, 2015 and accepted October 19, 2015.

Published online October 20, 2015
10.1021/acsnano.5b03565

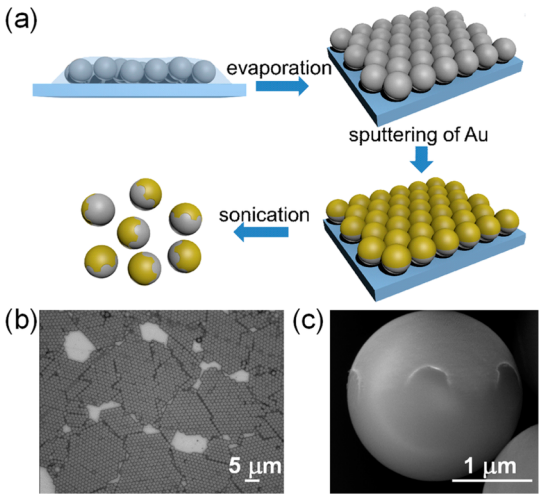

Figure 1. (a) Fabrication of patterned Janus particles. (b) Micrograph of a dried monolayer of polystyrene particles on a glass substrate before sputtering. (c) SEM image of a patterned Janus particle. The upper half of the particle is coated with gold.

hoppings of the particle center and reversals of rotational directions, which render them unviable for practical applications.[40]

In this article, we report experiments that achieve controlled stable rotation of a Janus particle in a linearly polarized optical trap by introducing patterned metal coatings through a simple procedure. Both the rate and the direction of the rotor can be flexibly controlled by adjusting the position or intensity of the focused laser beam. We show, through numerical calculations, that the patterned boundary line breaks the reflective symmetry of an ideal Janus particle, resulting in two stable configurations of lower symmetry for a particle in an optical trap, corresponding to two opposite rotational directions.

RESULTS AND DISCUSSION

Sulfonated polystyrene (PS) particles are synthesized using dispersion polymerization method.[41] The hydrodynamic diameters of the microspheres are determined by dynamic light scattering to be 3.0 μm, with a polydispersity of 2%. Janus particles are fabricated in a process illustrated in Figure 1a. First, a drop of ethanol diluted PS solution (0.01 mL) is deposited on a clean hydrophilic glass slide, using a micropipette. A thin liquid film is formed as the deposited solution rapidly spreads on the glass surface. The particles in the thin film aggregate into a monolayer of closely packed hexagonal structure after drying, as shown in Figure 1b, from the attraction induced by the menisci between particles during evaporation. Au is then sputtered on dried patches of PS particles, coating one hemisphere with ~5 nm of metal. Finally, these particles are resuspended in deionized water by sonification. An SEM image of redispersed Janus particle is shown in Figure 1c. One notable feature of these particles is that the boundary between the coated and uncoated surfaces is not a flat line parallel to the equator, but a wavy line with distinctive patterns (additional images are included in Figure S1 in Supporting Information). These patterns are obviously related to the close-packed hexagonal structure of the PS monolayer before sputtering, in which most particles are in contact with 6 neighbors. The average number of neighbors for the PS spheres before sputtering is measured to be 5.7, with 79% of the spheres having 6 contacting neighbors. The vertically sputtered gold covers less area around the points of contact between neighboring particles, leading to the concaved patterns on the dividing line.

An optical trap is formed by focusing a linearly polarized laser (λ = 1064 nm) through an objective with variable numerical aperture. The power of the laser is adjustable from 15 to 114 mW. In our experiments, over 30 individual Janus spheres are measured, ~80% of which exhibit observable rotations in an optical trap. A series of snapshots of clockwise and counterclockwise rotation of a Janus particle are shown in Figure 2, panels a and b, respectively (see Video S1 and Video S2). The brighter part of the sphere corresponds to the uncoated hemisphere of the polystyrene. The Au-coated hemisphere appears darker in the images, as it transmits less light. The center of the trap is fixed relative to the camera, indicated as a red cross in Figure 2.

Several remarkable features are observed for the rotating Janus particles in an optical trap. First, the particle is oriented in a way that the dividing line between the coated and uncoated surfaces can be clearly seen from the top. This orientation is different from that of a free Janus particle whose coated hemisphere is slightly heavier and tends to point in the direction of gravity. Second, the center of the optical trap is always on the polystyrene side of the sphere. And third, once a Janus particle begins to rotate in the optical trap, it maintains stable rotational direction until it is released. The initial rotational direction is determined by the way the trap approaches the particle, which can be switched by releasing the particle and recapturing it from the opposite side.

When a metal-coated Janus particle approaches an optical trap, the polystyrene side of the particle feels the intense gradient of electric field near the focal point of the laser and is attracted toward the trap center, as illustrated in Figure 3a. For an uncoated PS sphere, the trap center will coincide with the particle center. For a coated Janus particle, however, the Au-coated hemisphere strongly scatters the intense laser and is thus repelled from the optical center, shown as F_{rep} in Figure 3a. This repulsive scattering force shifts the sphere center away from the optical axis, leaving the uncoated side of the sphere in the laser trap. For a symmetrically coated Janus particle with six identical and evenly spaced patterns, the

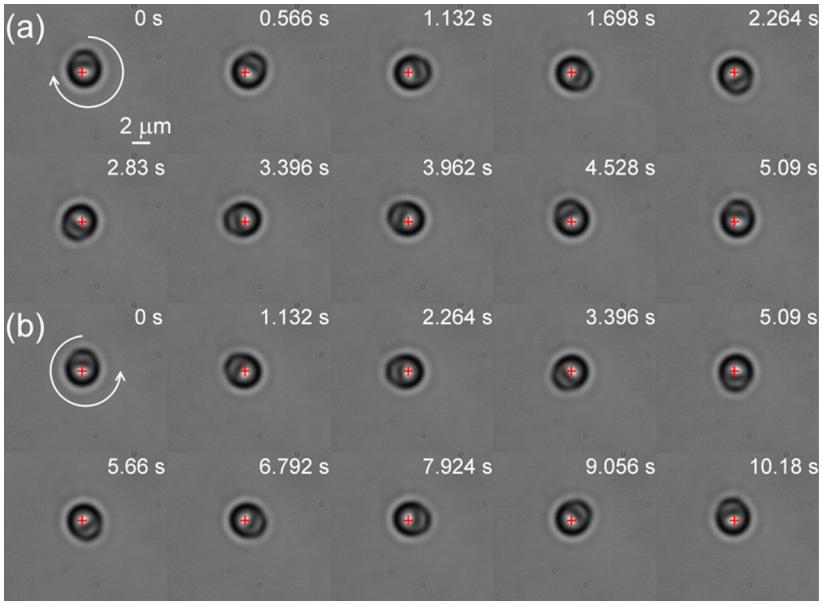

Figure 2. A series of snapshots showing a Janus particle rotating one complete circle. (a) Clockwise rotation, laser power *I* = 57 mW, objective NA = 0.7. (b) Counterclockwise rotation, laser power *I* = 28.5 mW, objective NA = 0.7. The position of the laser center is indicated by a red cross.

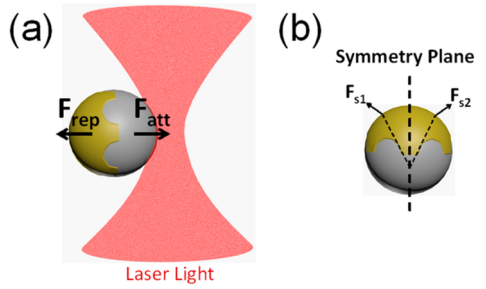

Figure 3. Janus particle in an optical trap. (a) Forces exerted on different hemispheres of a Janus particle and (b) symmetry of forces on the two hemispheres for optical trap located on the symmetry plane of the sphere.

optical center would naturally falls onto a symmetry plane that divides the particle into two identical hemispheres, as shown in Figure 3b. Under such configurations, laser-driven rotation along the optical axis is not possible, as any torque obtained from forces in the right hemisphere will be exactly canceled by an opposite torque from the mirror positions on the left hemisphere.

We extract the position and orientation of the rotating particle in an optical trap by analyzing the obtained digital images. Figure 4a shows the trajectory of the particle center relative to the trap center for a Janus particle under different conditions. The particle moves in nearly perfect circles around the trap, with no hopping events across the trap center. Two angles, α and θ, are introduced to describe the motion of a Janus particle. As illustrated in Figure 4b1, α is the angle between the center−center vector from the optical trap to the particle and the *x*-axis, and θ is the angle between the normal direction of the equator plane (from the polystyrene side to the Au-coated side) and the *x*-axis. α describes the translation of the particle mass center relative to the laser trap, while θ represents the spinning of the particle relative to its own center. When α and θ are equal, the rotation axis is on the symmetry plane of the sphere; otherwise. the axis is on either left or right side of the plane. Measured α and θ are plotted in Figure 4b2. The two angles are linearly correlated, suggesting that the translational motion and the spinning of the spheres are synchronized. The non-zero intercepts in Figure 4b2 show that optical center is not located on the symmetry plane. This relation becomes clear when the positions of the trap center are plotted in the reference frame of the particle in Figure 4c,d. The trap center is either on the left side of the symmetry plane (dashed vertical line) or on the right side of the plane. This deviation of the rotation axis from the symmetry plane dictates the rotational direction of the Janus sphere. When the trap is on the left side of the symmetry plane, the particle rotates counterclockwisely, and when the trap is on the right side of the plane, the particle rotates clockwisely. In practice, the correlation between the laser position and rotational direction can be employed to switch the rotational direction of a Janus particle. Stable rotations along axis of lower symmetry suggest that spontaneous symmetry breaking may have occurred in our system, which will be examined in detail in numerical analysis later.

The rate of rotation can be varied over a wide range by tuning the laser power or the numerical aperture (NA) of the objective lens. Figure 4e plots the rotational frequency of a Janus particle under different laser powers. The rotational rate increases almost linearly

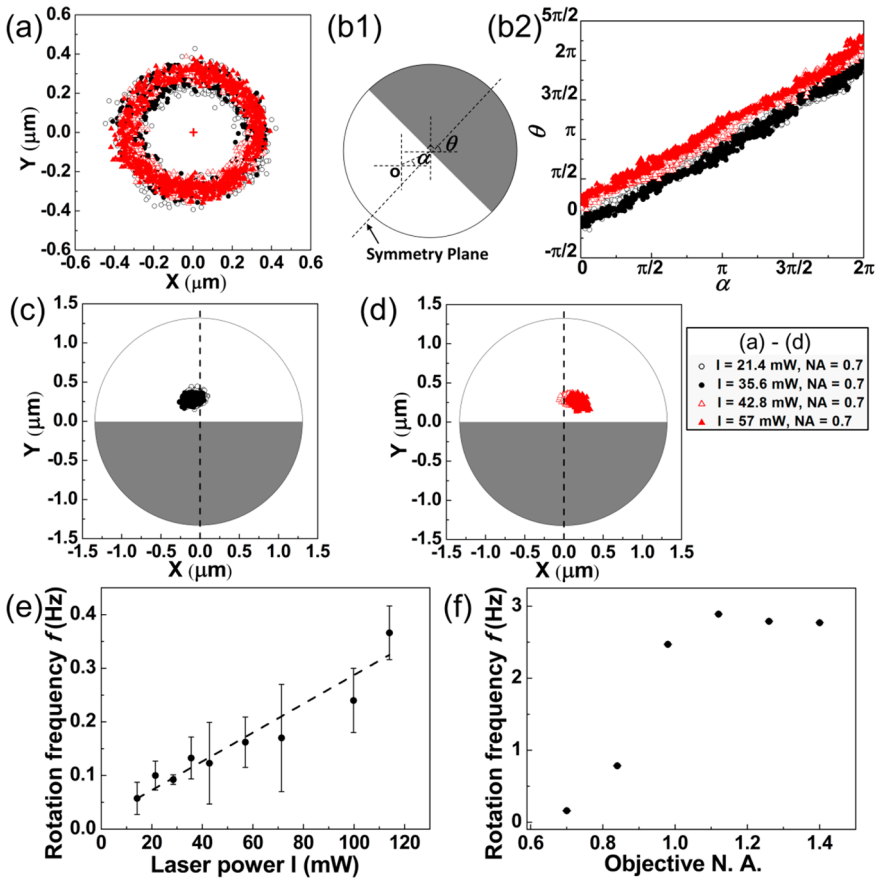

Figure 4. Rotation of a Janus particle in an optical trap. From (a) to (d), counterclockwise rotations are shown in black circles with *I* = 21.4 mW, NA = 0.7 (empty) and *I* = 35.6 mW, NA = 0.7 (filled); clockwise rotations are shown in red triangles with *I* = 42.8 mW, NA = 0.7 (empty) and *I* = 57 mW, NA = 0.7 (filled). (a) The position of the particle in the reference frame of the optical trap with the trap center as the origin of coordinates. The position of the laser center is indicated by a red cross. (b1) Definition of the orientational angles. The gray area represents the metal-coated hemisphere; the trap center is located at the origin, denoted by an o. (b2) Measured orientational angles of a Janus particle in an optical trap, θ as a function of α. (c) The positions of the beam center in the reference frame of the Janus particle for counterclockwise rotations. (d) The positions of the beam center in the reference frame of the Janus particle for clockwise rotations. (e) Rotation frequency of the Janus particle as a function of the laser power (with NA = 0.7); and (f) as a function of numerical aperture of the objective lens (with *I* = 57 mW).

with laser power. The numerical aperture, which determines the focusing angle of the laser trap, has more significant influence on the rotational rate. As plotted in Figure 4f, the rotational speed increases by an order of magnitude when the NA changes from 0.7 to 1.0 (also see Video S3 and Video S4) for a constant laser power of 57 mW. The rotational rate appears to reach a plateau for NA greater than 1.0.

To investigate the driving mechanism for the observed bistable rotation of Janus particles in an optical trap, we employ ray optics algorithms to calculate the force and torque generated by a focused laser on a Janus particle with patterned coatings. Details of the algorithm can be found in the Supporting Information. Briefly, by tracing the reflection, refraction, and absorption of an incident ray, an elementary force or torque can be evaluated at each point the ray encounters an interface on the particle. The overall force and torque exerted on a Janus particle can thus be obtained for arbitrary trap-particle configurations. Ray optics algorithm is a geometry-optics based method that is computationally inexpensive, thus suitable for fast searching in large parameter spaces.[42] We note that for particles whose sizes are comparable to the wavelength of incident laser light and with complex distribution of dielectric properties, this method may only be qualitatively reliable.[43]

The coordination system for the calculation is shown in Figure 5a. The trap center is fixed at the origin, and the laser beam propagates along the *z*-axis. The patterned Janus particle is initially oriented in such a way that the unit vector from the metal side to the polystyrene side is parallel to the *y*-axis. The particle is then scanned along the *x*-, *y*-, and *z*-axis in search of a position where the net force on the particles is zero. During the positional scan, the orientation of the particle is fixed. The torque is generally non-zero at the equilibrium position for forces. The sphere is then allowed to rotate around different axes until a stable configuration is reached. Rotations from the initial orientation around different axes are represented by γ_β, where $\beta = x, y,$ or z. At a stable configuration, the net

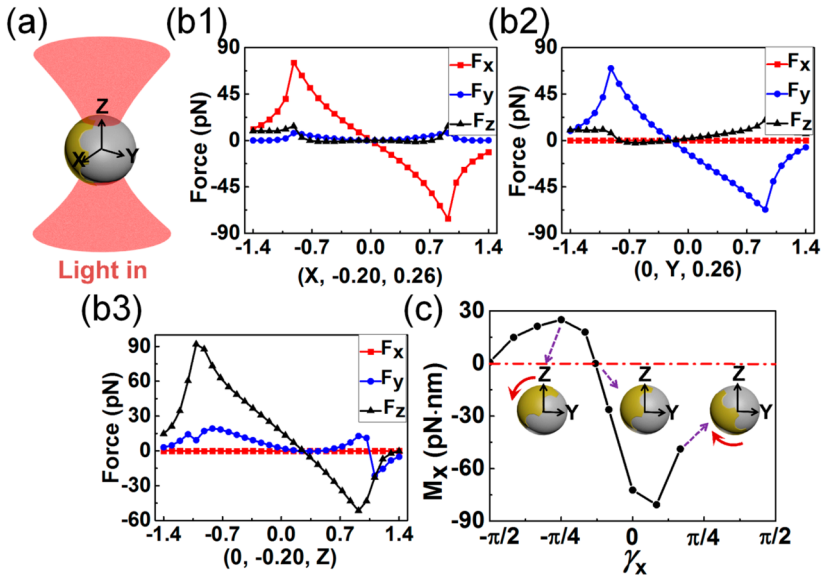

Figure 5. Numerical calculation for a symmetrically patterned Janus particle in an optical trap. (a) Schematic diagram of the coordinates for calculation setup and the initial configuration of the particle. (b1−b3) Calculated forces when the Janus particle is scanned along *x*, *y*, and *z* axis. Force components are represented by red (F_x), blue (F_y), and black (F_z). (c) Calculated torque along *x*-axis (M_x) as a function of the rotational angle along *x*-axis (γ_x), with the particle center fixed at the equilibrium position, and the rotational angle along *y*-axis (γ_y) is 0. The insets of (c) show the particle orientation at different γ_x (indicated by dashed arrows), with the red arrows showing the rotational direction under the calculated torque.

force on the particle is zero, and a small change of the particle position will result in a restoring force toward the equilibrium position (*i.e.*, the slope of the force−position curve is negative). At the same time, the direction of any remaining torque must be stable as the particle rotates under its influence.

We first examine the force and torque felt by a Janus particle with 6 evenly spaced identical concave patterns in an optical trap. The equilibrium coordinates for the particle center are found to be $r_e = (0, -0.20, 0.26)$. The calculated forces from the positional scans are plotted in Figure 5b1−b3, which show that r_e is a stable equilibrium position as the forces are zero for at all three directions, and the slope is negative when scanned along each axis. The negative *y*-coordinate of r_e indicates that the trap center is on the polystyrene side of the sphere, which is in agreement with experimental observations. The orientation of the sphere is determined by torque balance. Figure 5c plots the calculated torque when the particle is rotated around the *x*-axis. At equilibrium, the Janus particle is orientated at $\gamma_x = -\pi/9$, with the dividing plane between coated and uncoated surface nearly vertical to the *x*−*y* plane. This equilibrium orientation agrees with the experimental observation that the dividing line is always visible for the Janus particle in an optical trap. The equilibrium x coordinate, however, is zero, right on the symmetry plane of the particle, and the net torque for the particle is also zero.

Numerical calculations for the ideally patterned Janus particle in an optical trap confirm our qualitative analysis that the symmetry of the particle prohibits stable directional rotation. In experiments, however, the patterns on a Janus particle cannot be perfectly identical and evenly spaced. Many factors may contribute to an imperfect pattern of the coating, including particle polydispersity, the widths of particle separation, and the orientation of contacting particles. To take into account the effect of pattern asymmetry, we modify our particle model by decreasing the size of one of the 6 concaved patterns. This modification corresponds to a slightly larger separation between a Janus particle to one of its six neighbors. In Figure 6a1, this smaller concave, or "defect", is indicated by a blue arrow, and the other five are indicated by red arrows. The outlines of the regular and "defect" concaves are shown in Figure 6a2 for comparison. The ray optics algorithms are then applied to this modified Janus sphere model to search for stable configurations.

For the Janus particle with uneven patterns, numerical calculations reveal two nonequivalent equilibrium positions with the particle center located at $r_e = (0.0007, -0.1965, 0.2625)$ and $r_e = (-0.0007, -0.1965, 0.2625)$, on the two sides of the symmetry plane of the sphere. For these two equilibrium centers, net torques in the *z*-direction with values of 5.3 and −5.3 pN·nm are obtained, which drive the Janus sphere to rotate in the counterclockwise and clockwise directions around *z*-axis, respectively. Under dynamical rotations, the equilibrium positions of the trap center will shift slightly to provide the needed force for the translational motion of the particle center. The orientation angle in *x*-axis is nearly $-\pi/9$ with the dividing line being visible from the top, in agreement with experimental observations.

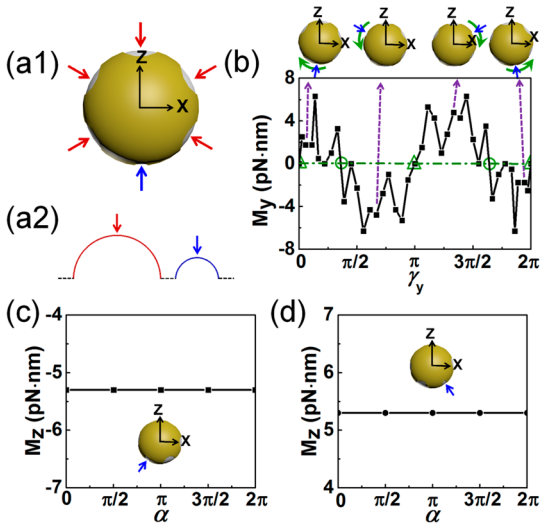

Figure 6. Calculations on an asymmetrically patterned Janus particle in an optical trap. (a1) The schematic of an asymmetrically patterned Janus particle. Red arrows point to regular concave patterns, and the blue arrow indicates the location of the "defect" pattern. (a2) The outlines of a regular concave pattern (red) and the "defect" concave (blue) (drawn to scale). (b) Calculated torque along *y*-axis (M_y) as a function of γ_y, with γ_x fixed at 0. Green circles indicate stable equilibrium angular positions, and green triangles indicate unstable equilibrium angular positions (shown by dashed arrows). Inset of (b) illustrates the angular position at different unbalanced angular positions, with blue arrows indicating the location of the defect, and green arrows showing the rotational direction from the non-zero torque. (c and d) The net torque (in *z*-axis direction) as a function of α (the same α in Figure 3b1) for counterclockwise (c) and clockwise rotations (d). The location of the defect is shown by a blue arrow in the insets of (c) and (d).

The deviation of the equilibrium positions from the symmetry plane is the direct result of torque balance around the *y*-axis. Figure 6b plots the torque for different angular positions when the particle is rotated around *y*-axis. A total of 4 angular positions are found where the torque changes sign, of which 2 are stable positions (large green circles). Any angular deviations from these two stable positions will be countered by a restoring torque as illustrated in Figure 6b. The two unstable angular positions (large green triangles), on the other hand, are two equivalent configurations separated by π. At these two positions, the $z-y$ plane divides the Janus particle into two identical hemispheres through the middle of the "defect". These two configurations, although highly symmetric, are unstable, as any angular deviation will be accelerated by a torque in the same direction. The barriers around the two stable angular positions fix the relative orientation between the Janus sphere and the trap center, which then give rise to a positive or negative net torque along the *z*-axis. Then, we calculate the net torque as the Janus sphere is rotated around the beam center and find that the torque is independent of angular positions of the Janus particle, providing a stable driving torque for continued rotations.

Thus, our calculations show that in the presence of uneven boundary lines, the system will settle at a stable state of lower symmetry, while the most symmetric states are unstable. These characteristics are the hallmarks of spontaneous symmetry breaking such as spontaneous magnetization, commonly found in condensed matter systems.[44] In fact, two separate symmetry breaking processes can be identified in our system. One of the processes is the orientation of the Janus sphere around *x*-axis illustrated in Figure 5c. In this case, the most symmetric configuration with the gold-coated hemisphere directly facing the illuminating laser is unstable. Instead, the particle assumes an orientation in which the gold cap is off-axis to the laser beam, where the torque from scattering forces is zero. The other symmetry breaking process is along the *y*-axis, which results the observed bistable rotation. The unevenly patterned Janus sphere can be separated into a perfectly patterned sphere and an extra cap of gold coating at the defect site. When placed at the most symmetric configuration, with the defect directly facing the incident light, the perfectly patterned sphere does not provide any torque, as our analysis showed earlier. The extra gold cap, on the other hand, experiences strong repulsive forces from the scattering laser. A small deviation from the symmetric configurations will create a net torque that drives the defect toward a position that minimizes the scattering forces. The insets of Figure 6c,d show that, at stable configurations, the "defect" is indeed off-axis with the optical beam.

So far our calculations have recovered the key experimental observations for a patterned Janus particle in an optical trap, and reveal that spontaneous symmetry breaking plays a critical role to the function of a Janus microrotor. Even though the calculation is performed on a very specific case of asymmetry, the underlying mechanisms are generally applicable.

To demonstrate that the shape of the dividing line between coated and uncoated surfaces is indeed an important factor to the generation of stable rotation of a Janus particle in an optical trap. We perform a control experiment on Janus particles whose dividing lines are flat. These particles are obtained by drying an extremely dilute suspension of polystyrene particles so that the particles are individually deposited on a glass slide without contacting neighbors. Details of this procedure are found in the Supporting Information. When captured by an optical trap, a Janus particle with flat dividing lines does not show any sustained directional rotation, only randomly vibrates near the trap center (see Video S5). The asymmetry of the dividing line is apparently not sufficient to create energy barriers that can maintain configurations for continued directional rotation.

CONCLUSION

We demonstrate a simple method to construct and operate a bistable microrotor consisting of a Janus

polystyrene colloidal particle with patterned gold coatings. When illuminated by a focused laser, the Janus particle can stably rotate around the optical axis. The Janus rotor permits easy control of both the rate and direction of rotation. Numerical analyses show that the observed directional rotation is the result of spontaneous symmetry breaking induced by the uneven patterns of metal coatings on the particles. Thus, instead of relying on precise fabrication of the device, our microrotor employs the inevitable imperfections on a Janus particle to realize stable and controllable rotation. Such microrotors have minimal requirements on the driving field and can be produced in large quantities at low costs. The reliability and flexibility of these microrotors make them ideal candidates for general applications in nano- and microdevices, such as micropumps, microvalves, or micromotors that provide power to other devices. After calibration, they can also function as microrheometers that probe local rheological properties of fluids.

METHODS

Materials. 2,2′-Azobis(isobutyronitrile) (AIBN, 98%, Sinopharm Chemical) was purified by recrystallization in ethanol. Styrene (98%, Sinopharm Chemical) was purified *via* passage through a basic alumina column to remove the inhibitor before use. Ethanol (95%, Beijing Tongguang), poly(vinylayrrolidone) (PVP, M_w = 30 000 g/mol, Sinopharm Chemical) and concentrated sulfuric acid (98%, Beijing Chemical) were used without further purification. Deionized water was obtained from a Milli-Q water purification system (Millipore, Bedford, MA).

Synthesis of Sulfonated Polystyrene Particles. Polystyrene particles were synthesized through a one-stage dispersion polymerization as described by Paine *et al.*[41] Briefly, 95 mL of ethanol and 1.0 g of PVP were added into a 250 mL three-neck reaction flask equipped with a condenser and a gas inlet. After a homogeneous solution was formed at room temperature, the flask was deoxygenated by bubbling nitrogen gas for 30 min. AIBN (0.14 g) was dissolved in 20 g of styrene and was then added into the reaction flask. The reaction continued for 24 h while the solution was agitated by a magnetic stirrer. The product was repeatedly centrifuged and washed with ethanol and deionized water. The powder of polystyrene microspheres was obtained by drying in vacuum at 30 °C. Then, 2.0 g of polystyrene powder and 80 mL of concentrated sulfuric acid were introduced to a round bottled flask. After ultrasonic dispersion, the sulfonation was allowed to take place at 40 °C under magnetic stirring for 3 h. After the product cooled to room temperature, it was again purified by repeated centrifugation and washing by deionized water.

Trapping and Driving the Janus Particle by Focused Laser. Janus particles/water suspension (1.3 μL) was loaded between two cover glasses and hermetically sealed using optical glue (Norland 65). The particles were confined to move freely in the $x-y$ planes, but not in the z-direction. An optical trap was generated by focusing infrared laser (Nd:YVO_4, Coherent Compass 1064 nm) through an oil-immersion objective (Leica, HCX PL APO, ×100, NA = 0.7−1.4). The maximum laser power after the objective was measured to be 114 mW. The images of the Janus particles were recorded by a CCD camera mounted on the microscope at 21 frames/s.

Characterization of the Motion of a Janus Particle in an Optical Trap. The position and orientation of the rotating Janus particles were determined using digital image analysis technique. To locate the center of the particle, a mask was used to locate the bright ring around the Janus particle, and the geometric center of the ring was determined to be the particle center. The orientation of the was is extracted by rotating the particle image on the first snapshot and searching for the rotating angle with the highest image correlation. The average rotation speed was measured using recorded video images by counting the number of rotation cycles in a given time. The error bars represent variations from different measurements.

Conflict of Interest: The authors declare no competing financial interest.

Supporting Information Available: The Supporting Information is available free of charge on the ACS Publications website at DOI: 10.1021/acsnano.5b03565.

Additional information on the experiment and details of calculations (PDF)
Video S1 (AVI)
Video S2 (AVI)
Video S3 (AVI)
Video S4 (AVI)
Video S5 (AVI)

Acknowledgment. The authors thank Lin Gu for providing the sputtering and SEM facilities for the fabrication and characterization of the Janus particles, Bao-Qin Chen for the laser grating fabrication, and Lin Gan for the thickness measurement of the gold coatings. K.C. acknowledges the support from the "The Recruitment Program of Global Youth Experts" of China. This work was supported by the MOST 973 Program (No. 2015CB856800) (K.C), and (No. 2013CB632704) (Z.Y.L.). We would also like to acknowledge the support from NSFC (11434017) (Z.Y.L.), (11474327) (K.C.) and (11404379) (M.C.Y.).

REFERENCES AND NOTES

1. Cabezon, E.; Lanza, V. F.; Arechaga, I. Membrane-associated Nanomotors for Macromolecular Transport. *Curr. Opin. Biotechnol.* **2012**, *23*, 537–544.
2. Derr, N.; Goodman, B.; Jungmann, R.; Leschziner, A.; Shih, W.; Reck-Peterson, S. Tug-of-War in Motor Protein Ensembles Revealed with a Programmable DNA Origami Scaffold. *Science* **2012**, *338*, 662–665.
3. Tischer, C.; Brunner, D.; Dogterom, M. Force- and Kinesin-8-Dependent Effects in the Spatial Regulation of Fission Yeast Microtubule Dynamics. *Mol. Syst. Biol.* **2009**, *5*, 250.
4. Gupta, M. L.; Carvalho, P.; Roof, D. M.; Pellman, D. Plus end-specific Depolymerase Activity of Kip3, a Kinesin-8 Protein, Explains its Role in Positioning the Yeast Mitotic Spindle. *Nat. Cell Biol.* **2006**, *8*, 913–923.
5. Várkuti, B. H.; Yang, Z.; Kintses, B.; Erdélyi, P.; Bárdos-Nagy, I.; Kovács, A. L.; Hári, P.; Kellermayer, M.; Vellai, T.; Málnási-Csizmadia, A. A Novel Actin Binding Site of Myosin Required for Effective Muscle Contraction. *Nat. Struct. Mol. Biol.* **2012**, *19*, 299–306.
6. George, N.; Irving, T.; Williams, C.; Daniel, T. The Cross-bridge Spring: Can Cool Muscles Store Elastic Energy?. *Science* **2013**, *340*, 1217–1220.
7. Wang, Y.; Fei, S.-t.; Byun, Y.-M.; Lammert, P. E.; Crespi, V. H.; Sen, A.; Mallouk, T. E. Dynamic Interactions between Fast Microscale Rotors. *J. Am. Chem. Soc.* **2009**, *131*, 9926–9927.
8. Gao, W.; Dong, R.; Thamphiwatana, S.; Li, J.; Gao, W.; Zhang, L.; Wang, J. Artificial Micromotors in the Mouse's Stomach: A Step Towards *In Vivo* Use of Synthetic Motors. *ACS Nano* **2015**, *9*, 117–123.
9. Wu, Z.; Li, T.; Li, J.; Gao, W.; Xu, T.; Christianson, C.; Gao, W.; Galarnyk, M.; He, Q.; Zhang, L. Turning Erythrocytes into Functional Micromotors. *ACS Nano* **2014**, *8*, 12041–12048.
10. Wu, Y.; Wu, Z.; Lin, X.; He, Q.; Li, J. Autonomous Movement of Controllable Assembled Janus Capsule Motors. *ACS Nano* **2012**, *6*, 10910–10916.

11. Gao, W.; Wang, J. Synthetic Micro/nanomotors in Drug Delivery. *Nanoscale* **2014**, *6*, 10486–10494.
12. Ruangsupapichat, N.; Pollard, M. M.; Harutyunyan, S. R.; Feringa, B. L. Reversing the Direction in a Light-Driven Rotary Molecular Motor. *Nat. Chem.* **2011**, *3*, 53–60.
13. Perera, U.; Ample, F.; Kersell, H.; Zhang, Y.; Vives, G.; Echeverria, J.; Grisolia, M.; Rapenne, G.; Joachim, C.; Hla, S. Controlled Clockwise and Anticlockwise Rotational Switching of a Molecular Motor. *Nat. Nanotechnol.* **2013**, *8*, 46–51.
14. Baraban, L.; Makarov, D.; Streubel, R.; Mönch, I.; Grimm, D.; Sanchez, S.; Schmidt, O. G. Catalytic Janus Motors on Microfluidic Chip: Deterministic Motion for Targeted Cargo Delivery. *ACS Nano* **2012**, *6*, 3383–3389.
15. Wang, J.; Gao, W. Nano/Microscale Motors: Biomedical Opportunities and Challenges. *ACS Nano* **2012**, *6*, 5745–5751.
16. Gibbs, J.; Kothari, S.; Saintillan, D.; Zhao, Y.-P. Geometrically Designing the Kinematic Behavior of Catalytic Nanomotors. *Nano Lett.* **2011**, *11*, 2543–2550.
17. Xia, H.; Wang, J.; Tian, Y.; Chen, Q. D.; Du, X. B.; Zhang, Y. L.; He, Y.; Sun, H. B. Ferrofluids for Fabrication of Remotely Controllable Micro-Nanomachines by Two-Photon Polymerization. *Adv. Mater.* **2010**, *22*, 3204–3207.
18. Yang, M.; Liu, R.; Ripoll, M.; Chen, K. A Microscale Thermophoretic Turbine Driven by External Diffusive Heat Flux. *Nanoscale* **2014**, *6*, 13550–13554.
19. Yang, M.; Ripoll, M. A Self-Propelled Thermophoretic Microgear. *Soft Matter* **2014**, *10*, 1006–1011.
20. Yang, M.; Ripoll, M.; Chen, K. Catalytic Microrotor Driven by Geometrical Asymmetry. *J. Chem. Phys.* **2015**, *142*, 054902.
21. Fan, D.; Zhu, F.; Cammarata, R.; Chien, C. Controllable High-speed Rotation of Nanowires. *Phys. Rev. Lett.* **2005**, *94*, 247208.
22. Kim, K.; Xu, X.; Guo, J.; Fan, D. Ultrahigh-speed Rotating Nanoelectromechanical System Devices Assembled from Nanoscale Building Blocks. *Nat. Commun.* **2014**, *5*, 3632.
23. Fan, D.; Zhu, F. Q.; Xu, X.; Cammarata, R. C.; Chien, C. Electronic Properties of Nanoentities Revealed by Electrically Driven Rotation. *Proc. Natl. Acad. Sci. U. S. A.* **2012**, *109*, 9309–9313.
24. Gao, W.; Kagan, D.; Pak, O. S.; Clawson, C.; Campuzano, S.; Chuluun-Erdene, E.; Shipton, E.; Fullerton, E. E.; Zhang, L.; Lauga, E. Cargo-Towing Fuel-Free Magnetic Nanoswimmers for Targeted Drug Delivery. *Small* **2012**, *8*, 460–467.
25. Gao, W.; Sattayasamitsathit, S.; Manesh, K. M.; Weihs, D.; Wang, J. Magnetically Powered Flexible Metal Nanowire Motors. *J. Am. Chem. Soc.* **2010**, *132*, 14403–14405.
26. Ghosh, A.; Fischer, P. Controlled Propulsion of Artificial Magnetic Nanostructured Propellers. *Nano Lett.* **2009**, *9*, 2243–2245.
27. Lehmuskero, A.; Ogier, R.; Gschneidtner, T.; Johansson, P.; Käll, M. Ultrafast Spinning of Gold Nanoparticles in Water using Circularly Polarized Light. *Nano Lett.* **2013**, *13*, 3129–3134.
28. Tsai, W.-Y.; Huang, J.-S.; Huang, C.-B. Selective Trapping or Rotation of Isotropic Dielectric Microparticles by Optical Near Field in a Plasmonic Archimedes Spiral. *Nano Lett.* **2014**, *14*, 547–552.
29. Wu, T.; Nieminen, T. A.; Mohanty, S.; Miotke, J.; Meyer, R. L.; Rubinsztein-Dunlop, H.; Berns, M. W. A Photon-Driven Micromotor can Direct Nerve Fibre Growth. *Nat. Photonics* **2012**, *6*, 62–67.
30. Friese, M.; Nieminen, T.; Heckenberg, N.; Rubinsztein-Dunlop, H. Optical Torque Controlled by Elliptical Polarization. *Opt. Lett.* **1998**, *23*, 1–3.
31. Arita, Y.; Mazilu, M.; Dholakia, K. Laser-Induced Rotation and Cooling of a Trapped Microgyroscope in Vacuum. *Nat. Commun.* **2013**, *4*, 2374.
32. Friese, M.; Nieminen, T.; Heckenberg, N.; Rubinsztein-Dunlop, H. Optical Alignment and Spinning of Laser-Trapped Microscopic Particles. *Nature* **1998**, *394*, 348–350.
33. Neale, S. L.; MacDonald, M. P.; Dholakia, K.; Krauss, T. F. All-Optical Control of Microfluidic Components Using Form Birefringence. *Nat. Mater.* **2005**, *4*, 530–533.
34. Angelsky, O.; Bekshaev, A. Y.; Maksimyak, P.; Maksimyak, A.; Mokhun, I.; Hanson, S. G.; Zenkova, C. Y.; Tyurin, A. Circular Motion of Particles Suspended in a Gaussian Beam with Circular Polarization Validates the Spin Part of the Internal Energy Flow. *Opt. Express* **2012**, *20*, 11351–11356.
35. Lin, X.-F.; Hu, G.-Q.; Chen, Q.-D.; Niu, L.-G.; Li, Q.-S.; Ostendorf, A.; Sun, H.-B. A Light-Driven Turbine-Like Micro-Rotor and Study on its Light-to-Mechanical Power Conversion Efficiency. *Appl. Phys. Lett.* **2012**, *101*, 113901.
36. Liu, M.; Zentgraf, T.; Liu, Y.; Bartal, G.; Zhang, X. Light-Driven Nanoscale Plasmonic Motors. *Nat. Nanotechnol.* **2010**, *5*, 570–573.
37. Higurashi, E.; Ukita, H.; Tanaka, H.; Ohguchi, O. Optically Induced Rotation of Anisotropic Micro-Objects Fabricated by Surface Micromachining. *Appl. Phys. Lett.* **1994**, *64*, 2209–2210.
38. Qian, B.; Montiel, D.; Bregulla, A.; Cichos, F.; Yang, H. Harnessing Thermal Fluctuations for Purposeful Activities: the Manipulation of Single Micro-Swimmers by Aadaptive Pphoton Nudging. *Chem. Sci.* **2013**, *4*, 1420–1429.
39. Jiang, H.-R.; Yoshinaga, N.; Sano, M. Active Motion of a Janus Particle by Self-Thermophoresis in a Defocused Laser Beam. *Phys. Rev. Lett.* **2010**, *105*, 268302.
40. Merkt, F.; Erbe, A.; Leiderer, P. Capped Colloids as Light-Mills in Optical Traps. *New J. Phys.* **2006**, *8*, 216.
41. Paine, A. J.; Luymes, W.; McNulty, J. Dispersion Polymerization of Styrene in Polar Solvents. 6. Influence of Reaction Parameters on Particle Size and Mmolecular Weight in Poly (N-vinylpyrrolidone)-Stabilized Reactions. *Macromolecules* **1990**, *23*, 3104–3109.
42. Ashkin, A. Forces of a Single-Beam Gradient Laser Trap on a Dielectric Sphere in the Ray Optics Regime. *Biophys. J.* **1992**, *61*, 569–582.
43. Jiang, Y.; Narushima, T.; Okamoto, H. Nonlinear Optical Effects in Trapping Nanoparticles with Femtosecond Pulses. *Nat. Phys.* **2010**, *6*, 1005–1009.
44. Pathria, R. K.; Beale, P. D. *Statistical Mechanics*, 3rd ed.; Elsevier: New York, 2011; pp 412.